Available online at www.sciencedirect.com

ScienceDirect

Advances in Space Research 77 (2026) 4901–4908

ADVANCES IN SPACE RESEARCH (a COSPAR publication)

www.elsevier.com/locate/asr

Improved attitude modeling for GPS III satellites in the eclipse season

Oliver Montenbruck [a,*], Bingbing Duan [b], Peter Steigenberger [a], Urs Hugentobler [b]

[a] Deutsches Zentrum für Luft- und Raumfahrt (DLR), German Space Operations Center (GSOC), Münchener Straße 20, 82234 Weßling, Germany
[b] Technische Universtät München (TUM), Arcisstr. 21, 80333 München, Germany

Received 25 November 2025; received in revised form 27 December 2025; accepted 30 December 2025
Available online 5 January 2026

Abstract

GNSS satellites traditionally apply a yaw steering attitude to keep their antenna pointing to the Earth while maintaining the solar panel rotation axis perpendicular to the Sun-spacecraft-Earth plane. During the eclipse season, i.e., in periods with low Sun elevation (β-angle) above the orbital plane, the idealized, nominal yaw steering typically results in angular rotation rates that exceed the capabilities of the momentum wheels for attitude changes. To cope with this issue, different types of rate-limited yaw steering laws are applied by GNSS satellite designers during noon and midnight turns in the eclipse season. Knowledge of the yaw steering profile is essential for a proper modeling of the antenna phase center offset from the center of mass as well as the phase wind-up. This makes it a prerequisite for precise orbit determination and time synchronization (ODTS) as well as precise point positioning (PPP). For GPS III satellites, however, no detailed attitude model has been published by the manufacturer so far. Instead, different substitutes are presently in use by the various analysis centers (ACs) of the International GNSS Service (IGS). Making use of the fact that attitude modeling errors are largely absorbed in the estimated clock offsets of the highly-stable GPS Rubidium Atomic Frequency Standards (RAFS), the performance of individual models is analyzed using precise clock products and associated attitude quaternions of individual IGS ACs. While partly masked by stochastic clock variations, use of the Jet Propulsion Laboratory (JPL) attitude quaternions yields a clearly reduced clock variance in the vicinity of noon and midnight turns when compared to alternatives such as the GPS IIR and IIF models considered by other ACs. Since JPL attitude quaternions are only published with delays and no specification of the underlying model has been released, we show that the JPL model can well be represented by a yaw steering law with an orbit-angle-dependent β-angle modification. This enables an analytical description of the GPS III attitude that can readily be used for ODTS and PPP applications and is suggested as a common GPS III attitude model for future IGS processing.

Keywords: GPS III; Yaw steering; Attitude; Noon/midnight turns; RAFS

1. Introduction

While orbiting the Earth, the inertial orientation of a GNSS satellite in medium Earth orbit (MEO) needs to be continuously changed such as to align the antenna boresight with the spacecraft-Earth direction. At the same time, a Sun-pointing orientation of the solar panels must be ensured to maximize the electrical energy output. These conditions are jointly met by rotating the GNSS satellite about the Earth-pointing axis such as to keep the solar panel rotation axis orthogonal to the Earth-satellite-Sun plane, while rotating the panels to fully face the Sun. The resulting orientation of the spacecraft body relative to the orbital and the Sun direction is illustrated in Fig. 1 and commonly designated as "nominal yaw steering". Irrespective of possibly different body axis conventions used by individual spacecraft manufacturers, the key body axes in this figure and the subsequent discussion are based on conventions of the International GNSS Service (IGS; Johnston

* Corresponding author.
E-mail address: oliver.montenbruck@dlr.de (O. Montenbruck).

https://doi.org/10.1016/j.asr.2025.12.111
0273-1177/

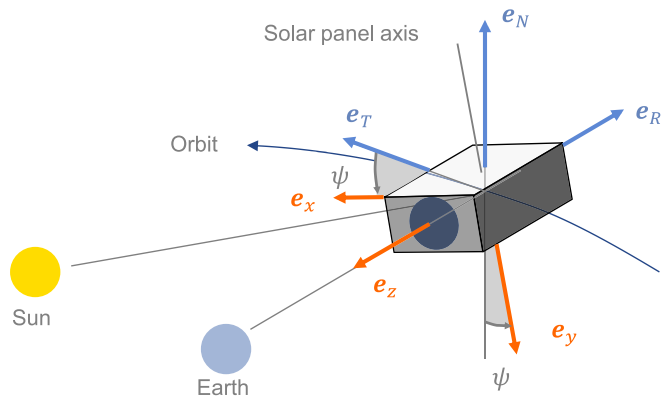

Fig. 1. Schematic view of the GPS III yaw steering. The yaw angle ψ describes the orientation of the spacecraft body frame with respect to the orbital frame with unit vectors $(\boldsymbol{e}_{\mathrm{R}}, \boldsymbol{e}_{\mathrm{T}}, \boldsymbol{e}_{\mathrm{N}})$ in radial, along-track, and orbit-normal direction. The assignment of the body axes $(\boldsymbol{e}_x, \boldsymbol{e}_y, \boldsymbol{e}_z)$ adopted in the drawing follows IGS axis conventions (Montenbruck et al., 2015) and corresponds to a sunlit $+x$-hemisphere.

et al., 2017), which enable a harmonized attitude description across different GNSSs and are further detailed in Montenbruck et al. (2015). Here, z and y designate the body axes parallel to the antenna boresight and the solar panel rotation axis, respectively. The x-axis, finally, completes a right-handed orthogonal system. The basic attitude requirements for GNSS satellites imply that one of the two body faces perpendicular to the x-axis is sunlit throughout an orbit, while the opposite panel is pointing to deep space. For thermal control purposes, the "hot" and "cool" side of the spacecraft are fixed by design and never altered during the attitude steering throughout the mission. Without loss of generality, a Sun-facing $+x$-axis is adopted in the IGS body axis conventions, while the $-x$-panel is continuously shaded in the nominal attitude.

As shown in Fig. 1, the GNSS attitude can fully be parameterized by the yaw-angle ψ between the along-track direction $\boldsymbol{e}_T$ and the $+x$-direction e_x. Following Bar-Sever (1996), the nominal yaw angle can be expressed as

$$\psi_{\mathrm{nom}} = \mathrm{atan2}(-\tan\beta, \sin\mu), \tag{1}$$

where μ denote the satellite's orbit angle counted from the local midnight line and β is the Sun elevation above the orbital plane (Kouba, 2009; Hugentobler and Montenbruck, 2017). Near the noon ($\mu = \pi$) and midnight epochs ($\mu = 0$) the nominal yaw angle amounts to $\psi = \pm\pi/2$ and its rate of change

$$\dot{\psi}_{\mathrm{nom}} = \dot{\mu}\frac{\tan\beta\cos\mu}{\sin^2\mu + \tan^2\beta} \tag{2}$$

reaches a maximum of

$$|\dot{\psi}|_{\mathrm{nom,max}} = \dot{\mu}/|\tan\beta| \tag{3}$$

with

$$\dot{\mu}_{\mathrm{GPS}} = \frac{2\pi}{43080\mathrm{s}} = 0.1458\ \mathrm{mrad/s}, \tag{4}$$

which grows with decreasing β-angle. Whenever the nominal yaw rate exceeds the spacecraft-specific hardware limitation for rapid yaw-slews during periods of low Sun elevation above the orbital plane, the nominal yaw steering can no longer be applied and a rate-limited yaw profile needs to be adopted, instead.

Proper knowledge of the GNSS satellite attitude is essential for an accurate modeling of pseudorange and carrier phase measurements in precise point positioning (PPP; Teunissen, 2021), where it affects both the modeled position of the antenna phase center as well as the phase wind-up effect (Wu et al., 1993). Within the orbit determination and time synchronization (ODTS; Weiss et al., 2017) of GNSS satellites, the orientation of the spacecraft body and solar panels furthermore affects the modeling of non-gravitational forces such as solar radiation pressure, Earth radiation pressure, and thermal radiation.

Over the years, rate-limited yaw models have been disclosed for a variety of GNSS satellite types or derived from observations using a reverse kinematic precise point positioning (reverse PPP) technique (Dilssner et al., 2011). Most types of GPS and GLONASS satellites maintain a constant yaw rate equal to the ceiling value over extended arcs of the rate-limited slew, but implement notably different concepts for reaching and ending the peak rate (Bar-Sever, 1996; Kouba, 2009; Dilssner et al., 2011; Kuang et al., 2017). Following the nomenclature of Strasser et al. (2021), these include "catch-up yaw steering", "shadow max yaw steering and recovery", "shadow max yaw steering and stop", "shadow constant yaw steering", and "centered max yaw steering". Symmetric yaw profiles relative to the noon or midnight epoch are only implemented in constant-rate GPS-IIF midnight turns, where the applied slew rate is adjusted to the duration of the Earth shadow transit, as well as GLONASS-M noon turns and GLONASS-K1/K2 noon and midnight turns (Kuang et al., 2017; Dilssner et al., 2011; Steigenberger et al., 2024).

As an alternative to maintaining a constant yaw rate for part of the slew, various types of "smoothed yaw steering" laws (Strasser et al., 2021) may be considered. A "dynamic yaw steering" (Ebert and Oesterlin, 2008; Zentgraf et al., 2006) has first been proposed for the GIOVE-B satellite in preparation of the European Galileo system. It modifies the nominal yaw steering by replacing the true β-angle with a time dependent value $\bar{\beta}(\beta, \mu)$, which keeps the corresponding yaw rate below the desired peak value and ensures continuous yaw rates and accelerations. Here, a weighting function depending on the orbit angle μ is used to smoothly transition between the actual β-angle and a desired threshold of $\beta_0 = \pm\dot{\mu}/|\omega|_{\mathrm{max}}$. A variant of that concept using a time-dependent cosine-weighting function has later been implemented in the Galileo In-Orbit Validation (IOV) satellites (GSC, 2017). For the Full Operational Capability (FOC), the yaw angle profile itself is described by a cosine function in time or orbit angle with a fixed period limiting the maximum required yaw rate to the design

values (GSC, 2017). As noted by Dilssner et al. (2018), the dynamic yaw steering law of Ebert and Oesterlin (2008) can also be used to describe the observed attitude during rate-limited yaw steering of selected BeiDou-2/3 satellites, even though the actual on-board algorithms have not been publicly disclosed.

Despite continued efforts for standardization and harmonization, the diversity and complexity of the rate-limited yaw steering concepts has resulted in various inconsistencies between specific implementations in use by individual analysis centers (ACs) of the IGS. Since the yaw model directly affects the estimated respective clock offset solution, users of IGS products would, ideally, require full knowledge of the AC-specific yaw model implementation applied in the product generation. For this purpose, the exchange of quaternion-based attitude data with a sufficiently dense sampling has been proposed and first been validated in the IGS repro3 reprocessing campaign by Loyer et al. (2021). Currently, attitude quaternions are routinely generated by selected IGS ACs including the Center for Orbit Determination in Europe (COD), the Helmholtz Centre for Geosciences (GFZ), the Centre National des Études Spatiales/ Collecte Localisation Satellites (GRG), the Jet Propulsion Laboratory (JPL), and Wuhan University (WUM) for their operational (OPS) or multi-GNSS experimental (MGX) product chains. The various attitude products provide the basis for a direct analysis of AC-specific modeling difference and have, e.g., been used in comparative studies of Liu et al. (2022),Yang et al. (2025), and Kuang et al. (2025).

While rate-limited yaw models supporting proper attitude modeling in the eclipse period have become available for most current GNSS satellite types, no such model is presently known for the latest generation of GPS satellites, i.e., GPS III (Marquis and Shaw, 2011). So far, no manufacturer information has been disclosed and the application of a reverse PPP is hampered by the near-zero offset of the GNSS antenna from the yaw-axis. In the absence of a dedicated yaw model, either a nominal yaw steering or the yaw steering model of the GPS IIR/-M satellites built by the same manufacturer or the IIF model are most widely assumed for GPS III by ACs of the IGS. As an exception, a non-standard, rate-limited yaw model is applied by JPL, which is designated as a "manufacturer model" in Geng et al. (2024), albeit without further references and explanations. While the underlying algorithm has not been disclosed, attitude quaternions representing the modeled attitude are publicly shared as part of the JPL0OPSFIN products for the IGS (Bertiger et al., 2020). These indicate a symmetric yaw angle profile with peak rates of about 0.09°/s during both noon and midnight turns that differs notably from both the IIR/-M and IIF profiles (Fig. 2).

To assess the quality and realism of the currently adopted GPS attitude models, we investigate the time series of estimated clock offsets in the periods of interest and assess their smoothness during relevant yaw slews in Section 2. Even though the clock products of a given AC have been determined with a specific yaw model, we can account for the impact of phase windup in the clock solution using an analytical correction and thus compute transformed GPS III clock offset solutions representative of any other yaw model. Throughout the considered test cases, use of the JPL attitude yields a better clock continuity and reduced variations compared to other models in current use by IGS ACs. To enable a wider use of the JPL attitude model without depending on the post-facto availability of JPL's quaternion product, an analytical model is presented, which closely matches the quaternion-based attitude profiles of GPS satellites in the eclipse season. The formulation of this yaw model and its properties are discussed in Section 3 and the model is proposed as a common standard for a harmonized ODTS and PPP processing within the IGS.

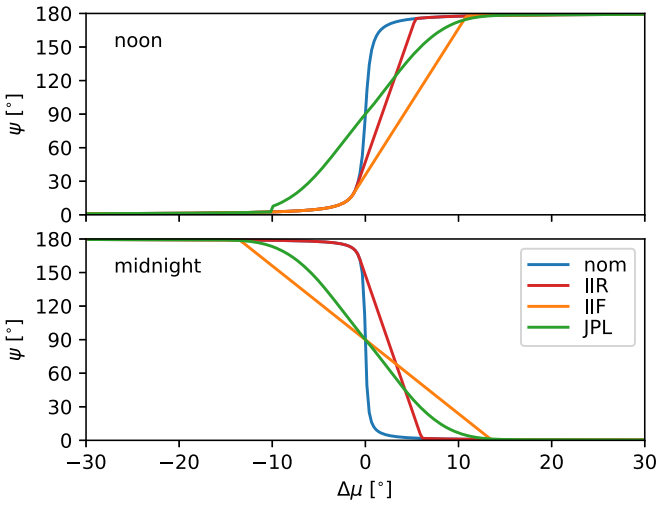

Fig. 2. Yaw angle profiles for noon (top) and midnight (bottom) yaw slews of GPS III satellites as considered by different IGS analysis centers.

2. Performance analysis of GPS III attitude quaternions

To evaluate the impact of different attitude models within the GNSS processing, we consider a tailored version of the observation model given in Hauschild (2017). Ignoring atmospheric range delays and other contributions without direct relevance for the present purpose, the carrier phase measurements can be described as

$$\varphi = ||\boldsymbol{r}^{\mathrm{sat,pc}} - \boldsymbol{r}_{\mathrm{rcv,pc}}|| + c \cdot (dt_{\mathrm{rcv}} - dt^{\mathrm{sat}}) + A + \omega\lambda. \quad (5)$$

Here $\boldsymbol{r}^{\mathrm{sat,pc}}$ and $\boldsymbol{r}_{\mathrm{rcv,pc}}$ denote the phase center positions of the transmitting satellite antenna and the receiving antenna, dt^{sat} and dt_{rcv} are the satellite and receiver clock offsets, c is the velocity of light, A is the carrier phase ambiguity (including integer multiples of the wavelength λ and fractional phase biases), and ω denotes the carrier phase wind-up (in cycles). Following Wu et al. (1993), the phase wind-up equals the accumulated angle

$$2\pi\omega = \angle(\boldsymbol{D}_{\mathrm{rcv}}, \boldsymbol{D}^{\mathrm{sat}}) \quad (6)$$

between the effective dipoles of $\boldsymbol{D}_{\rm rcv}$ and $\boldsymbol{D}^{\rm sat}$ of the receiver and transmitter antennas, which depend on the orientation of the antenna axes in space and are orthogonal to the line-of-sight unit vector $\boldsymbol{e}$ from the receiver to the satellite.

Taking into account the transmit antenna offset $\Delta\boldsymbol{r}^{\rm sat}_{\rm pco}$ between the phase center of the transmit antenna and the satellite center of mass (CoM), the observation model can be expressed as

$$\varphi = \rho + (\boldsymbol{E}(\psi)\boldsymbol{e})^T \Delta\boldsymbol{r}^{\rm sat}_{\rm pco} + c\cdot(dt_{\rm rcv} - dt^{\rm sat}) + A + \omega(\psi)\lambda, \tag{7}$$

where ρ is the range between the satellite CoM and the phase center of the receiver antenna, while $\boldsymbol{E}(\psi)$ describes the transformation from the terrestrial reference frame to the satellite antenna frame. Eq. (7) provides the basis for estimating the yaw angle within a reverse PPP approach, if the line-of-sight projection $(\boldsymbol{E}(\psi)\boldsymbol{e})^T\Delta\boldsymbol{r}^{\rm sat}_{\rm pco}$ of the PCO exhibits a sufficient variation with ψ. In practice, this requires phase center offsets $(\Delta x_{\rm pco}, \Delta y_{\rm pco})$ perpendicular to the antenna boresight axis at the level of one wavelength or larger. For GPS III satellites, on the other hand, these offsets amount to only 7 cm (Lockheed Martin, 2021). This limits the total range and phase change for a 180° yaw slew to just a few centimeters even for stations at large off-nadir angles and notably hampers the yaw-angle determination from carrier phase observations.

Besides the PCO contribution, the carrier phase model of Eq. (7) exhibits a secondary dependence on the yaw angle ψ related to the phase wind-up effect. However, this contribution is largely independent of the line-of-sight direction and the receiver location. As such, it is hardly observable even with a global network of monitoring stations and mostly indistinguishable from the satellite clock offset. Nevertheless, the estimated satellite clocks are directly affected by the applied yaw model and differences between the those models can indeed be recognized in a comparison of clock products from different ODTS providers.

For a quantitative description of the impact of yaw model differences on the estimated clock offset, we consider a homogeneously distributed station network for ODTS. Here, the average line-of-sight vector $\bar{\boldsymbol{e}} = -\boldsymbol{e}_z$ equals the unit vector along the anti-boresight direction. As a result, the mean contribution of a phase center offset perpendicular to the boresight direction vanishes and the resulting range contribution becomes independent of the yaw angle:

$$\overline{(\boldsymbol{E}(\psi)\boldsymbol{e})^T\Delta\boldsymbol{r}_{\rm pco}} = z_{\rm pco} = \text{const.} \tag{8}$$

At the same time, the global-average dipole vector

$$\overline{\boldsymbol{D}}^{\rm sat} = \boldsymbol{e}_x \tag{9}$$

matches the x-axis unit vector of the transmit antenna (and satellite body) frame. As such, differences $\Delta\psi$ in the applied yaw model directly map into a corresponding phase wind-up angle $\omega = \Delta\psi/(2\pi)$ and, finally, a difference

$$\Delta(cdt^{\rm sat}) = -\frac{\lambda\Delta\psi}{2\pi} \tag{10}$$

of the estimated clock offset (Loyer et al., 2021; Geng et al., 2024). Here, $\lambda = c/(f_{\rm L1}+f_{\rm L2}) \approx 0.107$ m denotes the effective wavelength of the ionosphere-free linear combination of phase observations at the L1 and L2 frequencies as used in the GPS clock offset estimation.

Making use of this relation, the impact of yaw model differences in the ODTS process may be assessed. Furthermore, clock products can be corrected after the fact and translated to a different yaw model if desired. To illustrate this concept, Fig. 3 compares representative clock offset time series of space vehicle number (SVN) G075 on March 3, 2025 obtained with different attitude models. The data are based on the 5-s clock solution of the COD0OPSFIN product (Dach et al., 2023), which substitutes a GPS IIR attitude model for the GPS III satellites. For assessing the influence of different attitude models on the clock solution, we apply Eq. (10) and translate the COD0OSFIN clocks from the IIR reference attitude to both the IIF attitude and JPL's GPS III model.

Even though the effect of different attitude models is partly masked by the stochastic clock variations of the GPS III Rubidium Atomic Frequency Standards (RAFS; Wu and Feess, 2000), both the time series and the associated Allan deviations (ADEV; Riley and Howe, 2008) provide clear evidence for the benefit of the JPL model. Both the IIF model and, even more, the IIR model show obvious ramps in the clock offsets during the central part of the yaw slews with amplitudes exceeding the level of natural clock variations. These are absent or at least largely diminished when using the JPL model in the clock offset computation. The JPL model also results in the lowest Allan deviation for correlation times τ in the range of 300 – 3000s, where the corrected ADEV closely follows the relation $\sigma_y(\tau) \approx 10^{-12}\cdot(\tau/\text{s})^{-1/2}$ observed at short correlation time intervals and outside the eclipse zones (Gianniou et al., 2023; Widczisk et al., 2026).

3. Analytical yaw-model for GPS III

The analysis of clock time series in the vicinity of the noon and midnight turns presented in the previous section provides strong evidence that the JPL attitude quaternions provide a better representation of the true yaw angle profile than alternative rate-limited models such as the IIR/IIR-M and IIF models. Most importantly, the JPL model for GPS III satellites applies notably lower yaw rates than those models, which results in a longer duration of the respective yaw slews. At the same time, the yaw profiles are roughly symmetric relative to the noon/midnight epochs and mostly identical profiles apply for noon and midnight turns.

Following the categories of Strasser et al. (2021), the JPL profiles represents a "smoothed yaw steering", in which the yaw rate varies (mostly) gradually over the entire

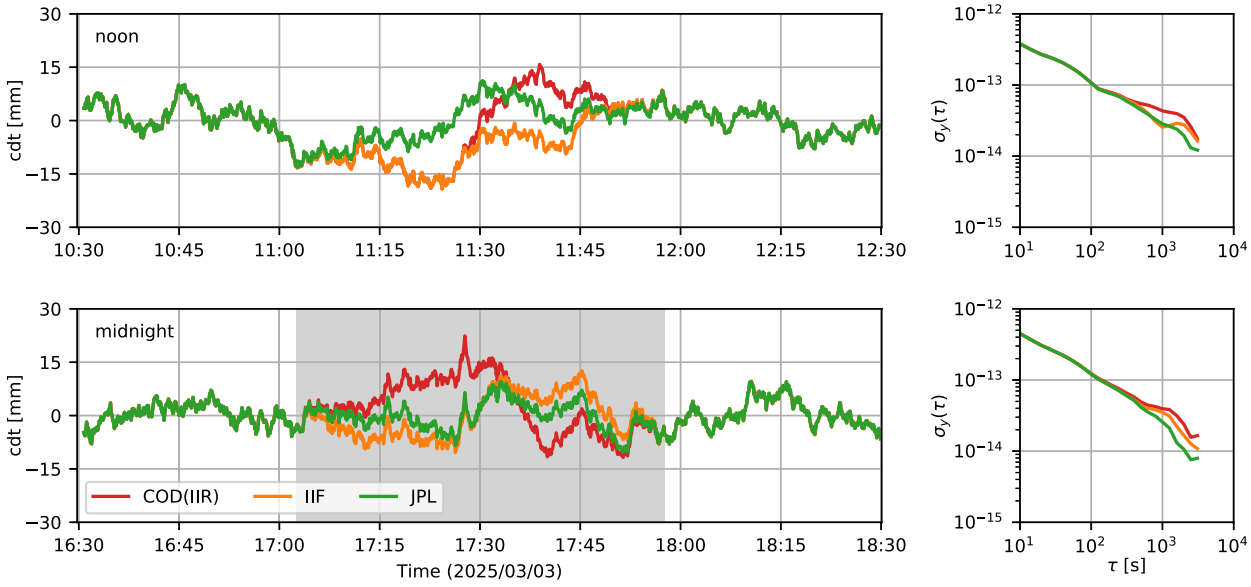

Fig. 3. Time series of estimated clock offsets after detrending with a second-order polynomial (left) and associated Allan deviations (right) of the GPS III satellite SVN G075 for a noon turn (top) and a midnight turn (bottom) at near-zero β-angle on March 3, 2025. Red lines represent the original clock solution of the COD0OPSFIN product based on a GPS IIR attitude model, orange lines the clock solution obtained after translation to the GPS IIF attitude, and green lines the clock solution after translation to the JPL attitude model for GPS III. The shaded area denotes the eclipse period in the vicinity of the midnight ($\mu = 0°$) epoch. (For interpretation of the references to colour in this figure legend, the reader is referred to the web version of this article.)

yaw turn rather than maintaining a constant peak rate in between distinct ramp-up and ramp-down phases. Actual GPS III yaw rates are illustrated in Fig. 4 for representative β-angles based on JPL attitude quaternions of SVN G074 in January 2025. The individual profiles are roughly bell-shaped and exhibit peak values of 0.08–0.09°/s. Here, it may be noted that the maximum yaw rate of 0.091°/s attained shortly before and after the noon/midnight epoch at near-zero β-angles is actually higher than the peak yaw rate of 0.082°/s for nominal yaw steering at the transition to the rate-limited zone.

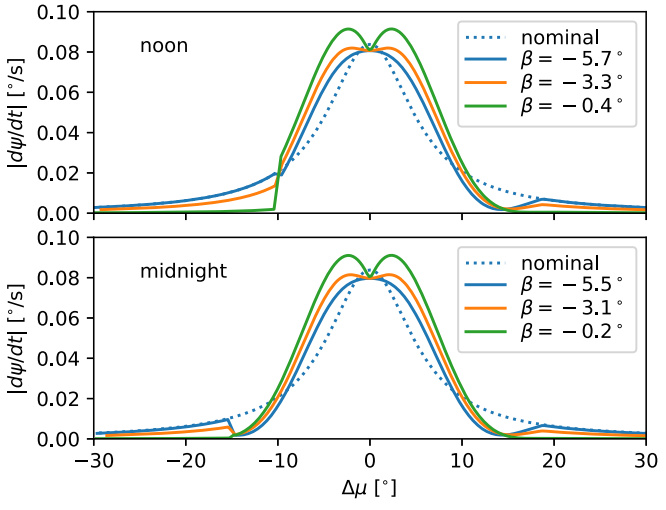

Fig. 4. Absolute yaw rates of the JPL model during rate-limited noon (top) and midnight (bottom) turns over a range of β-angles. For comparison, the dashed line shows the nominal yaw rate at $|\beta| = 5.7°$ close to the transition between the nominal-yaw regime and the rate-limited regime.

Based on inspection of the JPL quaternions for multiple GPS III satellites and eclipse seasons, a rate-limited yaw steering is applied for $|\beta| \lessapprox 5.8°$ during a period of about one hour around the noon/midnight epoch, while the nominal yaw steering is used outside the Sun-spacecraft-Earth collinearity region. Rate-limited yaw slews are performed over a period of roughly two to three weeks around the center of the eclipse period.

Prior to a noon turn, the transition from nominal yaw steering to the rate-limited mode in the JPL model takes place instantaneously at $\Delta\mu = -10°$ relative to noon (Fig. 4, top). The mode switch results in a discontinuity of the yaw angle by up to 7° and a step change in the yaw rate of up to 0.03°/s. Near the end of the rate-limited yaw turn, the yaw rate attains a near-zero value at about $\Delta\mu \approx +15°$. Thereafter, it increases again until it catches up with the nominal yaw steering at about $\Delta\mu \approx +19°$.

Prior to a midnight turn, the transition from nominal yaw steering to the rate-limited mode already takes place at $\Delta\mu = -15°$ relative to midnight (Fig. 4, bottom). Compared to the noon turn, discontinuities of the yaw angle and rate are generally smaller and amount to at less than about 1.5° and 0.01°/s. After the midnight turn, the yaw angle first drops to a near-zero value at about $\Delta\mu \approx +15°$ before gradually returning to the nominal values at $\Delta\mu \approx +19°$.

Among the currently known GNSS attitude models, the smoothed yaw steering models for the various generations

of Galileo satellites, i.e., GSTB-V2 (Ebert and Oesterlin, 2008; Zentgraf et al., 2006), IOV (GSC, 2017), and FOC (GSC, 2017) make use of roughly bell-shaped yaw-rate profiles and thus appear as the most promising candidates for an analytical approximation of the JPL attitude quaternions.

For use with GPS III, minor adaptions of the original yaw steering algorithms of the various blocks of Galileo satellites are considered. These facilitate a harmonized presentation of the three concepts and take care of the lower GPS III rotation rates as well as the wider range of β-angles requiring rate-limited yaw steering. The resulting formulation is based on the Sun direction unit vector

$$\boldsymbol{s} = \begin{pmatrix} s_x \\ s_y \\ s_z \end{pmatrix} = \begin{pmatrix} +\cos\beta\sin\mu \\ -\sin\beta \\ +\cos\beta\cos\mu \end{pmatrix} \tag{11}$$

in an orbital frame aligned with the along-track direction (x), the orbit normal (y), and the Earth direction (z). With these definitions, the yaw angle for nominal yaw steering can be expressed as

$$\psi_{\text{nom}} = \text{atan2}(s_y, s_x). \tag{12}$$

To keep the actual yaw rate below a desired threshold, the nominal yaw steering is replaced by an alternative yaw profile in a predefined collinearity region characterized by small values of $|s_x|$ and $|s_y|$. For a unified description of the three yaw steering profiles and their application to GPS III, we consider a rectangular collinearity region in the s_x/s_y-plane with limits γ_x and γ_y (Fig. 5). The rate-limited yaw steering is performed within this region, i.e., over a range $|\beta| < \sin^{-1}(\gamma_y)$ of Sun elevations and a range of orbit angle differences $|\Delta\mu| < \sin^{-1}(\gamma_x)$ relative to the noon/midnight epoch. For GPS III, limits of $\gamma_z = \sin(5.8^\circ)$ and $\gamma_x = \sin(15^\circ)$ are adopted in the subsequent comparison. Due to the lower peak rotation rates, the collinearity region for GPS III is notably larger than for the individual types of Galileo satellites. Therefore, a formulation in terms of the cartesian Sun vector is used

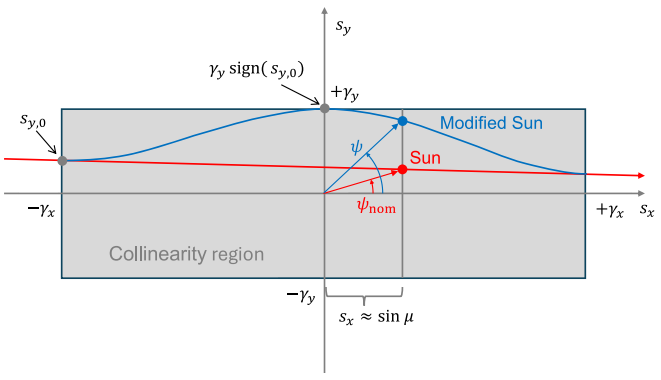

Fig. 5. Conceptual view of smoothed yaw steering for a midnight turn at $\beta < 0$.

in various places instead of plain angles in the GPS III adaptation of the individual algorithms.

In the GSTB-V2- and IOV-type models, the rate-limited slews are accomplished by replacing the true Sun elevation β by a modified value β^*, or, equivalently, s_y by s_y^*, whenever the true Sun vector is within the collinearity region. The rate-limited yaw angle can then be obtained as

$$\psi^* = \text{atan2}(s_y^*, s_x). \tag{13}$$

However, different approaches for the replacement values as a function of β and μ, or s_x and s_y, are employed in the two models. As a common feature, $|\beta^*|$ equals the limiting value $\beta_0 = \sin^{-1}(\gamma_y)$ at noon and midnight, which results in a corresponding yaw rate of

$$|\dot{\psi}| \approx \dot{\mu}/\gamma_y. \tag{14}$$

It may be noted, though, that this is not necessarily the peak rotation rate, since slightly larger rates may be encountered shortly before or after the noon/midnight epoch depending on the specific variation of s_y^* over time.

In the GSTB-V2-like model, a weighting function

$$f = \frac{1 - s_x^2}{1 + d \cdot s_x^2} \tag{15}$$

with a suitably chosen damping parameter d is used to obtain the modified value

$$s_y^* = (1.0 - f) \cdot s_y + f \cdot \text{sign}(s_{y,0}) \cdot \gamma_y, \tag{16}$$

where $s_{y,0}$ denotes the y-component of the Sun vector upon entry into the collinearity region. For application to GPS III, the overall shape of the JPL yaw-rate profile and its variation with β can best be described with a damping parameter of $d \approx 90$, which is roughly one third of the value originally suggested for GSTB-V2.

As an alternative, a cosine weighting function

$$g = \cos\left(\pi \frac{|s_x|}{\gamma_x}\right) \tag{17}$$

is used to compute the modified Sun vector component

$$s_y^* = 0.5 \cdot (1 + g) \cdot \text{sign}(s_{y,0}) \cdot \gamma_y + 0.5 \cdot (1 - g) \cdot s_y \tag{18}$$

in the IOV model.

For further simplification, the rate-limited yaw angle profile within the collinearity region is directly described by a harmonic profile

$$\psi^* = k \cdot \psi_0 + (1 - k) \cdot \frac{\pi}{2} \cdot \text{sign}(\psi_0) \cdot \tag{19}$$

with

$$k = \text{sign}(s_{x,0}) \cdot \sin\left(\frac{\pi}{2} \cdot \frac{s_x}{\gamma_x}\right) \tag{20}$$

in the FOC-type model. Compared to the original specification of the yaw profile for Galileo FOC satellites in GSC (2017)), Eqs. (19) and (20) have been adjusted in such a way as to enforce a symmetric profile relative to the

noon/midnight line at all β-angles in accord with the basic properties of the JPL GPS III model. Furthermore, the linear time dependence of the weighting factor k has been substituted by a linear dependence on s_x.

The rate profiles of the three Galileo-like yaw steering models for GPS III are illustrated in Fig. 6 for three selected noon turns covering the relevant range of β-angles. Compared to the JPL model, the cosine-shaped rate profile of the FOC-like models show a clearly inferior match than both the GSTB-V2- and IOV-type models. Near the limiting value of $|\beta| \approx \sin^{-1}\gamma_y$, those two models almost agree with each other, but do not reach the full width of the JPL rate profile in the central part of the yaw turn. At near-zero β-angles, the GSTB-V2 model also replicates the two side peaks of the JPL model, while the IOV model provides a better match in the early and later part of the slew.

For a quantitative comparison, Table 1 summarizes the root sum square (RMS) yaw angle differences of the three models with respect to the JPL attitude quaternions for three selected yaw turns over a period of ± 1 h or $\Delta\mu = [-30°, +30°]$ relative to the noon epoch. The best agreement is indeed found for the IOV-like model which achieves RMS errors of 2° to 3.5° over the entire zone of rate-limited yaw slews. Based on the above results, the IOV model with properly adapted collinearity zone limits ($\gamma_x = \sin(15°), \gamma_y = \sin(5.8°)$) is considered as the most suitable analytical model for approximating the actual JPL attitude quaternions for GPS III satellites.

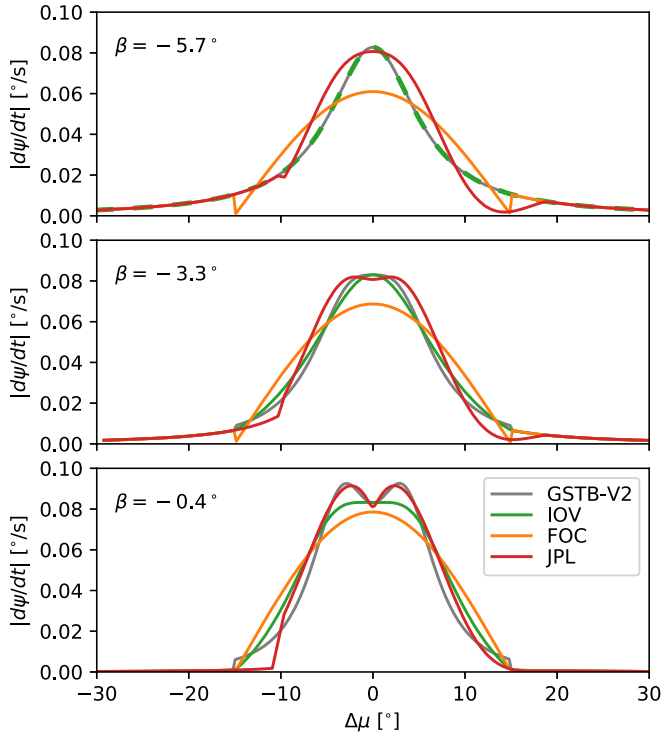

Fig. 6. Absolute yaw rates of different rate-limited yaw steering models as applied to GPS III noon turns at high (top), intermediate (center), and low (bottom) $|\beta|$-angles during the eclipse season of SVN G074 in January 2025. For the GSTB-V2-like model, a damping factor of $d = 90$ has been adopted. $\Delta\mu = \mu - 180°$ denotes the orbit angle offset from noon.

Table 1
Yaw angle differences (RMS) of Galileo-like attitude modes for GPS III and JPL attitude quaternions for noon turns of SVN G074 at different β-angles.

β	GSTB-V2	IOV	FOC
−5.7°	3.2°	3.2°	5.0°
−3.3°	2.5°	2.4°	4.2°
−0.4°	2.4°	1.9°	3.9°

4. Summary and conclusions

In the absence of a public manufacturer model for the rate-limited yaw steering of GPS III satellites, nominal yaw steering or rate-limited profiles of Block IIR and IIF satellites have been widely adopted so far by IGS ACs in the generation of precise orbit and clock products. While the publication of attitude quaternions along with the orbit and clock products ensures a consistent observation modeling by PPP users, concerns about the appropriateness of the substituted attitude models remain.

As an alternative to the aforementioned models, JPL is publishing GPS III attitude quaternions, which appear to represent an actual manufacturer model, even though no confirmation or public algorithm specification is presently available. Based on the analysis of precise clock products in the vicinity of noon/midnight turns near the center of the eclipse season and exploiting the good short term stability of the GPS III RAFS, we investigate the performance of the various attitude models for these satellites. The analysis provides strong evidence for a superior performance of the JPL model, which allows to recover the intrinsic oscillator stability during rate-limited slews in the estimated clock offsets.

As an alternative to the JPL attitude quaternions, which are only published after the fact, an analytical approximation is developed, which achieves an RMS error of less than 2° to 3.5° over the relevant range of β-angles. The model inherits the yaw steering concept of the Galileo IOV satellites, which replaces the true β-angle in the vicinity of the noon/midnight epoch by a modified value to keep the maximum yaw rate within specified limits. For use with GPS III, a modified collinearity zone extending ±15° in orbital longitude and ±5.8° is suggested. Compared to rate-limited yaw profiles employed in other spacecraft, the modified IOV model was found to provide the closest overall approximation of the JPL quaternions. It is therefore recommended as a transitional standard for use in OTDS and PPP with GPS III satellites. Up to a possible future release of the true GPS III yaw steering law, the IOV-like model presented here would facilitate a harmonized attitude modeling for IGS ACs and users of their products. This would largely reduce the dependence on

attitude quaternion products in PPP processing and simplify the generation of combined orbit/clock/bias products. Furthermore, use of the new model would enable generation of more precise GPS III clock solutions during the eclipse period.

Data availability

GNSS observations files and precise orbit/clock/attitude products as used in the study are publicly available from data centers of the IGS (e.g., https://cddis.nasa.gov/archive/gnss/data/).

Declaration of competing interest

The authors declare that they have no known competing financial interests or personal relationships that could have appeared to influence the work reported in this paper.

Acknowledgments

GNSS observation data and precise products as used in this study were kindly provided by the International GNSS Service (IGS). The support of all station providers, analysis centers and data centers is gratefully acknowledged.

References

Bar-Sever, Y.E., 1996. A new model for GPS yaw attitude. J. Geod. 70 (11), 714–723. https://doi.org/10.1007/BF00867149.

Bertiger, W., Bar-Sever, Y., Dorsey, A., et al., 2020. GipsyX/RTGx, a new tool set for space geodetic operations and research. Adv. Space Res. 66 (3), 469–489. https://doi.org/10.1016/j.asr.2020.04.015.

Dach, R., Schaer, S., Arnold, D. et al., 2023. CODE final product series for the IGS. http://www.aiub.unibe.ch/download/CODE. doi:10.48350/185744.

Dilssner, F., Laufer, G., Springer, T. et al., 2018. The BeiDou attitude model for continuous yawing MEO and IGSO spacecraft, EGU2018-15097. In: EGU General Assembly. URL: https://navigation-office.esa.int/attachments/32834482/1/EGU2018_Dilssner_Final.pdf.

Dilssner, F., Springer, T., Gienger, G., et al., 2011. The GLONASS-M satellite yaw-attitude model. Adv. Space Res. 47 (1), 160–171. https://doi.org/10.1016/j.asr.2010.09.007.

Ebert, K., Oesterlin, W., 2008. Dynamic yaw steering method for spacecraft. European patent specification EP 1526072B1.

Geng, J., Yan, Z., Wen, Q., et al., 2024. Integrated satellite clock and code/phase bias combination in the third IGS reprocessing campaign. GPS Solut. 28 (3), 150. https://doi.org/10.1007/s10291-024-01693-9.

Gianniou, M., Iliopoulou, O., Mendonidis, E. et al., 2023. A comparative performance assessment of Galileo and GPS satellite clocks. In: Proc. EUREF Symposoium 2023. URL: https://www.euref.eu/sites/default/files/symposia/2023Gothenburg/03-02-p-Gianniou.pdf.

GSC, 2017. Galileo satellite metadata.https://www.gsc-europa.eu/support-to-developers.

Hauschild, A., 2017. Basic observation equations. In: Teunissen, P., Montenbruck, O. (Eds.), Springer Handbook of Global Navigation Satellite Systems chapter, 19. Springer, Heidelberg, pp. 561–582. https://doi.org/10.1007/978-3-319-42928-1_19.

Hugentobler, U., Montenbruck, O., 2017. Satellite orbits and attitude. In: Teunissen, P., Montenbruck, O. (Eds.), Springer Handbook of Global Navigation Satellite Systems chapter, 3. Springer, pp. 59–90. https://doi.org/10.1007/978-3-319-42928-1_3.

Johnston, G., Riddell, A., Hausler, G., 2017. The International GNSS Service. In: Teunissen, P., Montenbruck, O. (Eds.), Springer Handbook of Global Navigation Satellite Systems chapter, 33. Springer, pp. 967–982. https://doi.org/10.1007/978-3-319-42928-1_33.

Kouba, J., 2009. A simplified yaw-attitude model for eclipsing GPS satellites. GPS Solut. 13 (1), 1–12. https://doi.org/10.1007/s10291-008-0092-1.

Kuang, D., Desai, S., Sibois, A., 2017. Observed features of GPS Block IIF satellite yaw maneuvers and corresponding modeling. GPS Solut. 21 (2), 739–745. https://doi.org/10.1007/s10291-016-0562-9.

Kuang, K., Guo, Z., Shen, Z., et al., 2025. Comprehensive assessment of GPS/BDS-3 MEO satellite attitude products from IGS analysis centers with analytical attitude model. Adv. Space Res. 76 (2), 686–698. https://doi.org/10.1016/j.asr.2024.10.040.

Liu, T., Chen, H., Jiang, W., et al., 2022. Assessing the exchanging satellite attitude quaternions from CNES/CLS and their application in the deep eclipse season. GPS Solut. 26 (1), 11. https://doi.org/10.1007/s10291-021-01197-w.

Lockheed Martin, 2021. Updated GPS-III antenna phase center values for SVN-74 through SVN-78 and timing group delay and inter-signal correction values as measured at the factory for SVN-78, Dececmber 2021. https://www.navcen.uscg.gov/sites/default/files/pdf/gps/GPSIII_APCs_SVNs_74_78_ISC_SVN78_Dec2021.pdf.

Loyer, S., Banville, S., Geng, J., et al., 2021. Exchanging satellite attitude quaternions for improved GNSS data processing consistency. Adv. Space Res. 68 (6), 2441–2452. https://doi.org/10.1016/j.asr.2021.04.049.

Marquis, W., Shaw, M., 2011. Design of the GPS III space vehicle. In: Proc. ION GNSS 2011, pp. 3067–3075.

Montenbruck, O., Schmid, R., Mercier, F., et al., 2015. GNSS satellite geometry and attitude models. Adv. Space Res. 56 (6), 1015–1029. https://doi.org/10.1016/j.asr.2015.06.019.

Riley, W., Howe, D., 2008. Handbook of Frequency Stability Analysis. National Institute of Standards and Technology. https://tsapps.nist.-gov/publi cation/get_pdf.cfm?pub_id=50505.

Steigenberger, P., Montenbruck, O., Hauschild, A., 2024. Antenna and attitude modeling of modernized GLONASS satellites. Adv. Space Res. 74 (7), 3045–3059. https://doi.org/10.1016/j.asr.2024.07.001.

Strasser, S., Banville, S., Kvas, A. et al., 2021. Comparison and generalization of GNSS satellite attitude models. In: EGU General Assembly 2021, EGU21-7825. doi:10.5194/egusphere-egu21-7825.

Teunissen, P.J., 2021. GNSS precise point positioning. In: Y.T.J. Morton, F. van Diggelen, J. J. J. Spilker, & B.W. Parkinson (Eds.), Position, Navigation, and Timing Technologies in the 21st Century: Integrated Satellite Navigation, Sensor Systems, and Civil Applications chapter 20. (pp. 503–528). Wiley IEEE Press volume 1. doi:10.1002/9781119458555.ch20.

Weiss, J., Steigenberger, P., Springer, T., 2017. Orbit and clock product generation. In: Teunissen, P., Montenbruck, O. (Eds.), Springer Handbook of Global Navigation Satellite Systems chapter 34, pp. 983–1010. doi:10.1007/978-3-319-42928-1_34.

Widczisk, J.S., Männel, B., Wickert, J., 2026. Investigations into highly stable GNSS ground and space clocks using a network of globally distributed H-maser stations. GPS Solut. 30 (1), 21. https://doi.org/10.1007/s10291-025-01986-7.

Wu, A., Feess, B., 2000. Development and evaluation of GPS space clocks for GPS III and beyond. In: Proc. 32th Annual Precise Time and Time Interval Systems and Applications Meeting, PTTI 2000, pp. 389–400.

Wu, J.-T., Wu, S.C., Hajj, G., et al., 1993. Effects of antenna orientation on GPS carrier phase. Manuscr. Geod. 18 (2), 91–98.

Yang, N., Xu, A., Xu, Z., et al., 2025. Effect of WHU/GFZ/CODE satellite attitude quaternion products on the GNSS kinematic PPP during the eclipse season. Adv. Space Res. 75 (1), 1–15. https://doi.org/10.1016/j.asr.2024.10.040.

Zentgraf, P., Fischer, H.-D., Kaffer, L., et al., 2006. AOC design and test for GSTB-V2B. In: Proc. ESA Guidance, Navigation and Control Systems Conference. volume SP606.